Giant hyperferroelectricity in LiZnSb and its origin

Shaohui Qiu, Steven Rhodes, and Huaxiang Fu

Phys. Rev. B **107**, 094108 — Published 17 March 2023

DOI: 10.1103/PhysRevB.107.094108

Giant hyperferroelectricity in LiZnSb and its origin

Shaohui Qiu[1], Steven Rhodes[2], and Huaxiang Fu[1]

[1]*Department of Physics, University of Arkansas, Fayetteville, Arkansas 72701, USA*

[2]*Department of Physics and Astronomy,*

Middle Tennessee State University, Murfreesboro, TN 37132, USA

Abstract

Hyperferroelectricity (HyFE) is an intriguing phenomenon in which spontaneous polarization persists under an open-circuit boundary condition (OCBC) despite the existence of depolarization field. However, small polarization and shallow well depth are found so far in most hyperferroelectric materials, which severely limits their applications. Using first-principles density functional theory, we report the discovery of a giant hyperferroelectricity in LiZbSb. The HyFE spontaneous polarization is shown to be remarkably large with P=0.282 C/m^2 under OCBC, which is one order of magnitude greater than the HyFE polarization in $LiNbO_3$. Furthermore, HyFE in LiZnSb is found to be exceptionally stable with a well depth of electric free energy ΔF=−332 meV, which makes LiZnSb a possible hyperferroelectric solid at room temperature. The origin of the giant hyperferroelectricity in LiZnSb is identified, and is attributed to the large mode effective charge of the soft longitudinal-optic phonon and the large high-frequency dielectric constant.

I. INTRODUCTION

Hyperferroelectricity (HyFE) is an interesting phenomenon of both fundamental and technological importance[1–3]. Differing from improper ferroelectrics (with the dominating structural instability occurring at the zone boundary)[4–7], materials with HyFE are a class of *proper* ferroelectrics (FE) in which ferroelectric instability originates from the soft phonons at the zone center. When proper FEs are under an open-circuit boundary condition (OCBC), the strong depolarization field tends to suppress ferroelectricity[8,9]. Intriguingly, HyFEs are able to maintain polar instability even under OCBC (despite the existence of depolarization field), which explains why HyFEs are fundamentally interesting[10].

Technologically, HyFEs can be potentially very useful in device miniaturization; for instance, the persisting polarization in HyFE thin films allows the FE memories to be smaller, which increases the storage density[11,12]. HyFEs may also possess unusual properties such as polarization tri-stability[13] and negative longitudinal piezoelectric coefficients[14]. Furthermore, HyFEs can be utilized (in heterostructures) to tune the properties of other functional materials such as topological insulators or superconductors.

HyFE has been reported to exist in hexagonal ABC-type semiconducting FEs such as LiBeSb[1], and in $LiBO_3$ compounds (where B can be V, Nb, Ta, and Os)[3]. Furthermore, HyFE was also shown to be metastable in $LiNbO_3$ under OCBC[13].

Despite the profound importance of HyFE, many fundamental challenges nevertheless remain in the field of HyFE. More specifically, (i) the spontaneous polarization under OCBC, found so far in many HyFEs, turns out to be tiny and not practically useful. For example, the HyFE polarization in LiBeSb is merely 0.02 C/m^2 under OCBC, which is more than twenty times smaller than the value of 0.59 C/m^2 of the same solid under a short-circuit boundary condition (SCBC)[1]. Similarly, in $LiNbO_3$ under OCBC, the HyFE polarization was reported to be 0.023 C/m^2, which is drastically reduced from the polarization of 0.768 C/m^2 in $LiNbO_3$ under SCBC[13]. The tiny HyFE polarization under OCBC poses an outstanding obstacle to the technological use of hyperferroelectricity. It is thus fundamentally important to search for HyFE materials of large polarization under OCBC. (ii) The well depth of hyperferroelectricity is detrimentally small, and consequently, the HyFE phase is stable only at very low temperatures. For instance, the free-energy well depth of the HyFE phase in $LiNbO_3$ under OCBC is only -1.9 meV, which is two orders of magnitude smaller than the

FE well depth of -227 meV under SCBC[13]. Thermal fluctuation can thus easily eliminate the hyperferroelectricity in $LiNbO_3$. Therefore, seeking the hyperferroelectricity that is stable under room temperature is of critical significance. (iii) HyFE defies the conventional wisdom, by possessing ferroelectricity despite the strong depolarization field. It is thus profoundly important to identify the origin on why HyFE exists—and even better, to discover the mechanism that can lead to strong HyFE with large polarization.

In this paper, we investigate the hyperferroelectricity in LiZnSb using frist-principles density functional theory. LiZnSb has been experimentally synthesized[15], and exhibits interesting properties such as superior thermoelectric conductivity[16]. We determine the HyFE polarization and well depth using a rigorous approach based on the electric free-energy under OCBC[17]. When a solid possesses hyperferroelectricity, the electric free energy under OCBC should, by definition, exhibit a minimum at a structure configuration of nonzero polarization.

We find that (i) a giant HyFE polarization exists in LiZnSb under -2% compressive inplane strain, and the magnitude of polarization is 0.282 C/m^2 under an *open-circuit* boundary condition, which is rather remarkable since this magnitude of polarization under OCBC is comparable to the polarization of 0.21 C/m^2 in prototypical ferroelectric $BaTiO_3$ under a *short-circuit* boundary condition[18]. (ii) The hyperferroelectricity in LiZnSb is discovered to be unusually stable, with a well depth of the electric free-energy being -332 meV. It indicates that the HyFE phase in LiZnSb is stable even under room temperature. (iii) The physical origin responsible for the giant hyperferroelectricity is shown to stem from two facts: the mode effective charge of the soft longitudinal-optic (LO) phonon is large in LiZnSb, and LiZnSb is close to be metallic with a large high-frequency dielectric constant. This finding also provides a useful guideline in order to search for new HyFE materials. (iv) Moreover, we reveal that hyperferroelectricity under OCBC responds to the inplane strain in an interestingly different manner than ferroelectricity under SCBC.

II. THEORETICAL METHODS

We employ the density functional theory (DFT) within the local density approximation (LDA)[19] to calculate the total (internal) energy, atomic force, cell stress, and the optimal structure, as implemented in Quantum Espresso[20,21]. Norm-conserving pseudopotentials of

the Troullier-Martins type is generated to replace the effects of core electrons[22,23]. Spin-orbit coupling is included in the calculations. The cutoff energy for plane-wave expansion of the single-particle wavefunctions is 120 Ry, which is tested to be sufficient. 6×6×4 Monkhorst-Pack k-mesh is used. A combination of three different methods are used to investigate the HyFE properties in LiZnSb. These methods are described as follows.

(i) The linear-response density functional perturbation theory (DFPT)[24–27] is used to study the lattice vibration and phonon modes. Phonon frequencies and eigenvectors are calculated by solving the secular equation $\det\left|\frac{1}{\sqrt{M_i M_j}}C_{i\alpha,j\beta}(\vec{q}) - \omega^2(\vec{q})\right| = 0$, where $C(\vec{q})$ is the force-constant matrix, ω is eigen-frequency, i and j are atomic indices, and α and β are the indices of Cartesian directions[28]. $C(\vec{q}) = C^a + C^{na}$ includes both the analytic part C^a and non-analytic part C^{na}[26]. The analytic part applies when there is no macroscopic electric field (i.e., when the system is under SCBC); C^a can be directly calculated using DFPT[25,26]. The non-analytic part comes from the interaction between lattice vibration and the macroscopic electric field, e.g., when the system is under OCBC. C^{na} is computed[26] as $C^{na}_{i\alpha,j\beta}(\vec{q}) = \frac{4\pi}{\Omega}e^2\frac{(\vec{q}\cdot Z_i)_\alpha(\vec{q}\cdot Z_j)_\beta}{\vec{q}\cdot\Sigma_\infty\cdot\vec{q}}$, where Z_i is the Born effective-charge tensor of atom i, and Σ_∞ is the high-frequency dielectric tensor due to the electronic response.

Since HyFE is related to soft modes and structural instability under OCBC[1–3], we begin with the paraelectric (PE) phase of LiZnSb, and optimize the atomic positions and cell structure while constraining it to be centro-symmetric. We then compute the zone-center phonon modes. The existence of a soft longitudinal-optic (LO) phonon in the PE phase indicates that the system is unstable under OCBC[1,2]. Nevertheless, the existence of soft LO phonon does not guarantee that the system is HyFE[13].

(ii) The electric free-energy approach[17] is used to determine whether (or not) HyFE exists in a solid. Once a zone-center soft LO phonon is determined, we then vary the atomic configuration using the vibration eigen-displacement $|\vec{u}_i>$ of this soft LO phonon, according to $\vec{r}_i(\lambda) = \vec{r}^{\,c}_i + \lambda c\vec{u}_i$, where $\{\vec{r}^{\,c}_i\}$ is the configuration of the PE phase, λ is the control parameter, and c is the lattice constant along the polarization direction.

The electric free-energy of a polar solid under a finite electric field E is defined[29] as $F = U - \Omega\left[P\cdot E + \frac{1}{2}\epsilon_0\chi_\infty E^2\right]$, which U is the internal energy, Ω the unit-cell volume, P the electric polarization, and $\chi_\infty = \Sigma^{33}_\infty - 1$ is the component of high-frequency dielectric permittivity. Here, both P and E are along the polar direction, and therefore the vector

notation is dropped. Using the free energy, one obtains the total polarization under a finite electric field as $P_{\rm tot} = -\frac{1}{\Omega}\frac{\partial F}{\partial E} = P + \epsilon_0\chi_\infty E$. In this equation, the electronic contribution to the total polarization (due to the field-induced wavefunction distortion) is included in the second term via high-frequency dielectric permittivity χ_∞. The ionic contribution is included in the first term (which is the Berry-phase polarization for *new* atomic positions after ions move). Therefore, the dielectric permittivity from ions is included in the free energy via polarization P and need not be accounted again. Using the vanishing electric displacement D=0 under OCBC, the electric free energy along the LO configuration path can be analytically determined as[17],

$$F(\lambda) = U(\lambda) + \Omega(\lambda)\frac{1+\frac{1}{2}\chi_\infty(\lambda)}{\epsilon_0[1+\chi_\infty(\lambda)]^2}P^2(\lambda)\,. \tag{1}$$

The second term in Eq.(1) is the energy cost due to the existence of depolarization field, and will be denoted as the depolarization energy $U_{\rm dp}(\lambda)$. By definition, a solid will be HyFE if the electric free-energy $F(\lambda)$ has a minimum at nonzero λ (i.e., at a configuration with nonzero polarization).

(iii) The electric polarization P in Eq.(1) is computed using the modern theory of polarization via the geometric Berry-phase approach[30,31]. Microscopic understanding of electric polarization can be further obtained using the theory of polarization structure[32].

III. RESULTS AND DISCUSSIONS

A. Structural and electronic properties of LiZnSb

The centro-symmetric PE phase of LiZnSb has P6$_3$/*mmc* symmetry, and its unit cell is shown in Fig.1(a), where Zn and Sb atoms are located on the same plane, and Li atoms occupy the intercalated positions. Polar LiZnSb (i.e., the FE phase) exhibits a LiGaGe structure with P6$_3$*mc* group symmetry, where Zn and Sb atoms occupy the sites of the wurtzite sublattices. The unit cell of the FE phase of LiZnSb is shown in Fig.1(b). The atomic positions and spontaneous polarization in FE LiZnSb were reported previously[33,34], but hyperferroelectric properties were not investigated in these studies.

The lattice constants obtained in our calculations are a=4.392 Å and c=7.490 Å for the PE phase of LiZnSb, where atoms are located at Li (0, 0, 0), Zn (2/3, 1/3, 1/4), and Sb

(1/3, 2/3, 1/4). For the FE phase of LiZnSb, our calculated lattice constants are a=4.355 Å and c=7.073 Å, which agree well with the values a=4.376 Å and c=7.081 Å in Ref.33, as well as with the results a=4.341 Å and c=6.962 Å in Ref.34. Atomic positions of FE LiZnSb are determined to be Li (0, 0, 0), Zn (2/3, 1/3, 0.342), and Sb (1/3, 2/3, 0.224) in our calculations, which are in good agreement with other studies (see Table I for comparison). Furthermore, our calculated electric polarization for FE LiZnSb under SCBC is 0.544 C/m^2, and our calculated depth of the FE double well is -0.776 eV. These values are consistent with the electric polarization of 0.56 C/m^2 and FE well depth of -0.8 eV in another study[33]. All these results show that our calculations are rather reliable.

Since hyperferroelectricity often occurs near the PE phase[1] and requires the knowledge of structural instability of soft LO phonon in the PE phase[13], we thus examine the PE LiZnSb in greater details. The calculated band structure of PE LiZnSb is shown in Fig.2(a). Interestingly we find that LiZnSb in the PE phase is metallic (or semimetal). Specifically, Fig.2(a) reveals that, near the zone-center Γ point, the top valence band and the bottom conduction band cross the Fermi energy [see the enlarged band structure in the bottom-right of Fig.2(a)], showing that the system is indeed metallic.

Strictly speaking, the metallic nature of PE LiZnSb does not allow us to investigate polarization and hyperferroelectricity, since the modern theory of polarization via the Berry's-phase approach requires that the system must remain to be insulating when it adiabatically moves along the path between the PE phase and the FE phase[30,31], in order for the electric polarization to be meaningfully defined. In metallic systems, the electric polarization, Born effective charges, and the LO/TO splitting are thus ill-defined[35,36], which prevents the investigation of the LO phonon and hyperferroelectricity under OCBC.

To drive the system out of the metallic state, we decide to apply the biaxial compressive inplane strain to LiZnSb. The band structure of PE LiZnSb under a -2% inplane strain is given in the left of Fig.2(b), showing that a direct band gap notably opens at Γ point. To further confirm that the system is insulating, we compute the density of states (DOS) across the full Brillouin zone (instead of the high-symmetry $\vec{k}$ paths as chosen in the band structure), and the obtained DOS is depicted in the right of Fig.2(b). Our calculated DOS reveals that there is a sizable band gap of $\sim$0.3 eV between the fully occupied valence states and the unoccupied conduction states, demonstrating that LiZnSb under a -2% inplane strain is indeed an insulator. Moreover, we also examine other magnitudes of compressive

inplane strains, ranging from -1% to -6%. We find (see the Appendix for details) that the LiZnSb solids under the considered range of compressive strains are all insulators, with the band gap varying from 0.10 eV to 0.45 eV, which thus allows us to investigate the HyFE properties. In the following, we will largely focus on LiZnSb under the -2% inplane strain, unless specified otherwise.

B. Giant hyperferroelectricity in LiZnSb

Existence of soft LO phonon was previously demonstrated to be an important and necessary (although not sufficient) condition for the emergence of HyFE[13]. We thus first perform linear-response calculations and determine the soft modes in PE LiZnSb under a -2% inplane strain. When LiZnSb is under SCBC (i.e., there is no macroscopic electric field and the non-analytic C^{na} contribution to the force-constant matrix is not included), we find two soft modes in PE LiZnSb: one is the polar $A_{2u}(TO_1)$ mode at frequency $\omega = 107i$ cm^{-1}, and the other is the non-polar B_{1g} mode at frequency $\omega = 67.8i$ cm^{-1}. The phonon eigenvectors of these two modes are given in Fig.1(c) and Fig.1(d), respectively. We see that (i) for the $A_{2u}(TO_1)$ mode in Fig.1(c), Zn atoms move upward while Sb atoms move downward, and both types of atoms have large vibration amplitudes; this mode is thus polar. Meanwhile, the Li vibration contribution is rather small. (ii) For the B_{1g} mode in Fig.1(d), the displacements of two Zn atoms in the unit cell are opposite, so are the displacements of two Sb atoms. B_{1g} is thus non-polar with no contribution from Li atoms.

When LiZnSb is under OCBC (i.e., when non-analytic C^{na} contribution is included), we find that the polar LO mode, $A_{2u}(LO_1)$, remains soft with imaginary frequency $\omega = 90.6i$ cm^{-1}, which indicates a structural instability under OCBC and a (possible) existence of HyFE. The phonon eigenvector of $A_{2u}(LO_1)$ is shown in Fig.1(e). Interestingly, compared to the transverse $A_{2u}(TO_1)$ mode in Fig.1(c), the longitudinal $A_{2u}(LO_1)$ mode in Fig.1(e) exhibits a (drastically) enhanced displacement from Li atoms, while the Zn and Sb displacements remain large. Therefore, Li atoms play an important role in forming the soft LO mode. Our calculations also show that, under OCBC, the frequency of the non-polar B_{1g} mode remains almost unchanged at $\omega = 68.2i$ cm^{-1}, which is not surprising since this mode is non-polar and does not interact with the macroscopic electric field.

After finding that $A_{2u}(LO_1)$ is soft in LiZnSb under a -2% inplane strain, we compute

the electric free energy F for the configuration path along the eigendisplacement direction of this soft mode. If F exhibits a minimum at a configuration of nonzero polarization, then by definition the system is HyFE. The calculated free-energy $F(\lambda)$ of LiZnSb under OCBC is depicted in Fig. 3(a), where the internal energy $U(\lambda)$ and the depolarization energy $U_{\rm dp}(\lambda)$ are also plotted for comparison. Fig.3(a) shows that, as λ deviates from zero, the free energy F starts to decrease, reaches a minimum at λ=$\pm$0.22, and then increases [see the curve of solid dots in Fig.3(a)]. Our results in Fig.3(a) hence reveal that LiZnSb at the PE configuration (i.e., λ=0) possesses a higher energy and is unstable under OCBC, and instead, LiZnSb prefers to be HyFE at nonzero λ. We thus find that LiZnSb is HyFE. We denote the configuration of LiZnSb at optimal λ=$\pm$0.22 as the LO-induced HyFE phase.

Importantly, Fig.3(a) further reveals that the free-energy well depth is $\Delta F_{\rm HyFE}$=$-$332 meV, which is remarkably large. In fact, this HyFE well depth in LiZnSb is more than *one hundred times* deeper than the HyFE well depth of -1.9 meV reported in $LiNbO_3$[13]. Furthermore, it is also worth pointing out that the *hyperferroelectric* well depth of LiZnSb under an *open-circuit* boundary condition is comparable to the ferroelectric well depth (about -200 meV) of bulk $PbTiO_3$ under a *short-circuit* boundary condition[37]. This tells us that (i) the hyperferroelectricity in LiZnSb is indeed very stable, and (ii) Since the ferroelectric Curie temperature of bulk $PbTiO_3$ is 493 °C, LiZnSb is thus likely to be hyperferroelectric at room temperature, which is appealing because it does not require cooling.

We find that the large depth of the HyFE free-energy well in LiZnSb is caused by the combination of a *deep* well of the internal energy U and a *small* depolarization energy $U_{\rm dp}$. As shown in Fig.3(a), at optimal λ=0.22, U is -0.537 eV, and meanwhile, $U_{\rm dp}$ is small and merely 0.205 eV, which gives rise to a strongly negative value of -0.332 eV in free energy F. Furthermore, we also calculate the electric free-energy along the configuration path of the non-polar B_{1g} mode, and find that the lowest free energy is ΔF=$-$150 meV, which is significantly higher than $\Delta F_{\rm HyFE}$=$-$332 meV of the LO-induced HyFE phase. This confirms that the ground state of LiZnSb is indeed HyFE under OCBC.

We also calculate the electric polarization of the HyFE phase under OCBC, using the modern theory of polarization via the geometrical Berry-phase approach[30,31]. At optimal λ=0.22, the magnitude of the HyFE polarization under OCBC is found to be $P_{\rm HyFE}$=0.282 C/m^2, which is gigantic. Note that this HyFE polarization is about 10 times larger than the $P_{\rm HyFE}$ value of $\sim$0.023 C/m^2 reported in LiBeSe[1] as well as in $LiNbO_3$[13]. As a matter of

fact, the HyFE polarization in LiZnSb under *open-circuit* boundary condition is remarkably comparable to the polarization of 0.21 C/m^2 in bulk ferroelectric $BaTiO_3$ under *short-circuit* boundary condition[18], despite that there is a strong depolarization field in LiZnSb. This large HyFE polarization is very attractive since it shall open many possibilities for hyperferroelectric applications; for instance, the HyFE polarization can be utilized to control the transport properties of semiconductors, superconductors, and/or topological insulators by forming interfaces or heterostructures.

C. Origin of the large and stable HyFE in LiZnSb

With the discovery of a giant polarization under OCBC and attractively stable hyperferroelectricity in LiZnSb, we now attempt to provide the physical origin of these interesting phenomena. We find that the strong hyperferroelectricity in LiZnSb can be attributed to two key quantities: (i) a large mode effective charge (MEC) of soft LO phonon, and (ii) a large high-frequency dielectric constant ϵ_∞ (i.e., from the electronic contribution). Here, the Σ_∞^{33} component of the high-frequency dielectric tensor is abbreviated as ϵ_∞.

We first find that a large mode effective charge is important in order to generate a large HyFE polarization. For an arbitrary phonon mode with normalized eigendisplacement $u_{i\beta}^{n\vec{q}}$, the mode-specific effective charge $\widetilde{Z}_\alpha^{n\vec{q}}$ is defined as[13]

$$\widetilde{Z}_\alpha^{n\vec{q}} = \sum_{i\beta} Z_{i,\alpha\beta}^* u_{i\beta}^{n\vec{q}} \ , \tag{2}$$

where n is the index of phonon branch, $\vec{q}$ the phonon wave vector, i the atom index, Z_i^* the dynamic Born effective-charge tensor of atom i, and α and β are the indices of Cartesian directions. Note that, after the summation over β in Eq.(2), $\widetilde{Z}_\alpha^{n\vec{q}}$ is a vector (not a tensor). Using the definition of MEC, it is straightforward to show that the HyFE polarization is directly proportional to MEC as $\Delta P_\alpha = \frac{1}{\Omega}\widetilde{Z}_\alpha^{n\vec{q}}\, c\, \Delta\lambda$, where c is the c-axis lattice constant. A large MEC will thus generate a large HyFE polarization. The most important component of MEC is the $\widetilde{Z}_3$ component along the polarization direction. We quantitatively calculate the $\widetilde{Z}_3$ value for the soft longitudinal-optic $A_{2u}(LO_1)$ mode in LiZnSb under -2% strain, and the obtained $\widetilde{Z}_3$ value is 2.59. To illustrate whether this value is large or small, we compare it to the $\widetilde{Z}_3$ value (merely 0.39) of soft LO mode in $LiNbO_3$[13]. We see that the $\widetilde{Z}_3$ value in LiZnSb is more than 600% larger than the value in $LiNbO_3$, which is one key reason why

the HyFE polarization in LiZnSb is large[38].

To demonstrate the importance of the high-frequency dielectric constant ϵ_∞, we artificially reduce the ϵ_∞ value by a factor of 1/3 (as well as by a factor of 1/4), and then recalculate the electric free energy F along the $A_{2u}(LO_1)$ configuration path. The calculated free energies are given in Fig. 3(b) and Fig. 3(c). Fig. 3(b) shows that, when the dielectric constant is changed to 1/3 of the original value, the free-energy well depth sharply decreases to ΔF=−33.4 meV, which is much smaller than the original value ΔF=−332 meV in Fig.3(a). And furthermore, the optimal λ of the free energy in Fig. 3(b) is also significantly reduced to λ=0.12, as compared to λ=0.22 in Fig.3(a). Since the HyFE polarization is directly proportional to the optimal λ, we thus see from Fig. 3(b) that, when ϵ_∞ is reduced, both the HyFE instability and the HyFE polarization are drastically weakened. When the dielectric constant ϵ_∞ is further reduced to 1/4 of the original value in Fig.3(c), we notice that the minimum of the electric free energy is no longer located at a nonzero λ. Instead, it is located at λ=0, and the PE phase becomes most stable under OCBC. Therefore the system is not HyFE. The calculation results in Fig. 3(b) and Fig. 3(c) thus demonstrate that the large dielectric constant ϵ_∞ in LiZnSb is indeed important.

It is rather intuitive to understand why both MEC and ϵ_∞ are important in order to produce strong HyFE. First, to generate large P_{HyFE} polarization, a large $\widetilde{Z}_3$ of soft LO phonon is needed since P_{HyFE} is proportional to $\widetilde{Z}_3$. Meanwhile, a large P_{HyFE} tends to (detrimentally) give rise to a large depolarization energy U_{dp}, which reduces the well depth ΔF of the HyFE free energy and weakens the HyFE instability. To reduce U_{dp} while maintaining a large P_{HyFE}, large ϵ_∞ is thus needed since U_{dp} is inversely proportional to ϵ_∞ according to Eq.(1)[39].

Our finding that large high-frequency dielectric constant ϵ_∞ is beneficial to generate strong HyFE also provides useful guide for searching new HyFE materials. Since large ϵ_∞ is often associated with small electronic band gap[40], new HyFE materials with strong HyFE should thus have a small band gap and a large mode effective charge of soft LO phonon.

We recognize that materials of small band gap tend to have a low dielectric breakdown electric field. It is thus helpful to estimate the hyperferroelectricity-switching electric field E_s and the dielectric breakdown electric field E_b in LiZnSb. Considering the facts that (i) the free-energy barrier (∼0.3 eV) of LiZnSb under OCBC is comparable to the internal-energy barrier (∼0.2 eV) of $PbTiO_3$ under SCBC, and (ii) the (intrinsic) switching electric field

in $PbTiO_3$ thin film is on the order of 10^7 V/m in experiment[41], it is thus reasonable that the intrinsic switching electric field E_s of the hyperferroelectricity in LiZnSb under OCBC will be also on the order of 10^7 V/m. Note that the extrinsic switching field will be one or two orders of magnitude smaller than the intrinsic switching field, since the nucleation of opposite domain is easier due to the existence of defect or domain wall. Real E_s may thus be considerably lower than the value estimated above. Meanwhile, the breakdown electric field E_b of LiZnSb can be estimated using $\frac{1}{\epsilon_r}E_b\, d = E_g$, where ϵ_r=30 is the relative zero-frequency dielectric constant, E_g≈0.3 eV is the band gap, and d is the film thickness. For d=20 nm LiZnSb film under OCBC, the breakdown field E_b is estimated to be 4.5×10^8 V/m, which is significantly higher than the switching field E_s. Therefore, it is possible that the hypeferroelectricity in LiZnSb can be switched. Furthermore, we recognize that the band gap (and thus the dielectric breakdown field) can be enlarged by strain, pressure, and/or quantum confinement.

There is subtle and important difference between hyperferroelectrics and polar metals, although the band gap of LiZnSb is small. Hyperferroelectrics require the existence of soft LO modes (and this soft LO mode often needs to have a large mode effective charge). In contrast, polar metals may not possess soft LO modes and are thus not hyperferroelectric, even if strain opens the band gap. For instance, doping a small amount of free carriers into $PbTiO_3$ may make it to become polar metal. But $PbTiO_3$ does not possess a soft LO mode, and is thus not hyperferroelectric.

One intriguing question centers on the role of Li atoms in hyperferroelectricity. To determine the role of Li atoms, we consider LiZnSb under a −2% strain at the optimal configuration of λ=0.22, and we constrain the displacement of Li atoms in the soft $A_{2u}(LO_1)$ mode to be zero (namely the Li atoms are fixed in positions). We then calculate the internal energy U, polarization P under OCBC, depolarization energy $U_{\rm dp}$, and free energy F. By comparing the values of these quantities with their counterparts (which are obtained when Li atoms are not constrained), we can quantitatively determine how Li atoms affect hyperferroelectricity. We obtain U=−0.577 eV, P=0.416 C/m^2, $U_{\rm dp}$=0.426 eV, and F=−0.151 eV for the Li-constrained system, as compared to U=−0.537 eV, P=0.259 C/m^2, $U_{\rm dp}$=0.205 eV, and F=−0.332 eV for Li-unconstrained system. We thus see that, by allowing Li atoms to move, the depolarization energy $U_{\rm dp}$ decreases drastically by more than 50% from 0.426 eV in the Li-constrained system to merely 0.205 eV in the Li-unconstrained system, due

to the fact that polarization P is significantly smaller in the latter. As a consequence, the free energy F is lowered considerably in the Li-unconstrained system, which stabilizes the hyperferroelectricity. Therefore, the Li atoms play an important role to stabilize hyperferroelectricity in LiZnSb by decreasing the polarization (and thus the depolarization energy) under OCBC. This is indeed consistent with the soft $A_{2u}(LO_1)$ mode in Fig.1(e), where the Li atoms move opposite to the Zn atoms (thus opposite to the direction of polarization).

D. Strain effects on HyFE

After revealing the origin of strong HyFE in LiZnSb, we now go one step further and investigate how the HyFE polarization—and the free-energy well depth—can be tuned by inplane strain. It is previously demonstrated that inplane strain alters *ferroelectricity* under SCBC[42–46]. However, the knowledge cannot be naively applied to *hyperferroelectricity* under OCBC, since the (strong) depolarization field plays a critical role on HyFE under OCBC (but not on FE under SCBC). Therefore, it remains intriguing to investigate how the HyFE properties under OCBC depend on the inplane strain. Furthermore, it is also interesting to examine how the response of HyFE under OCBC to the inplane strain may differ from (or resemble) that of FE under SCBC.

The calculated HyFE polarizations in LiZnSb under OCBC are given in Fig.4(a) for different inplane strains. For comparison, we also show in Fig.4(a) our calculated results on the FE polarization under SCBC. Fig.4(a) tells us that the FE polarization under SCBC increases monotonously as strain η varies from 0% to -6% [see the empty triangles in Fig.4(a)], which is not surprising[42–45]. However, and interestingly, for the HyFE polarization (P_{HyFE}) under OCBC, the behavior drastically differs: P_{HyFE} first *decreases* from 0.292 C/m^2 to 0.276 C/m^2 when strain changes from -1% to -3% (thus yielding a negative piezoelectric coefficient[46]), and then increases from 0.277 C/m^2 to 0.303 C/m^2 when strain varies from -4% to -6% [see the solid dots in Fig.4(a)]. P_{HyFE} thus depends on the inplane strain in a non-monotonous manner. Therefore, Fig.4(a) reveals one important outcome, that is, the hyperferroelectric polarization responds to the inplane strain very differently from the ferroelectric polarization. Also notably, for every inplane strain within the considered strain range in Fig.4(a), the HyFE polarization is found to be large and around 0.28 C/m^2, which is useful for technological applications.

We like to point out that, for unstrained LiZnSb, although the PE phase is metallic, it may still be possible to determine the hyperferroelectric P_{HyFE} polarization as follows. We start with the PE LiZnSb and move atoms along the nonpolar B_{1g} mode to a configuration where LiZnSb becomes insulating and meanwhile possesses an unstable LO mode. This insulating atomic configuration is still nonpolar and is used as a zero reference to calculate polarization. We then move atoms along the unstable LO mode and find the most stable hyperferroelectric phase. Using this approach we obtain the P_{HyFE} polarization in unstrained LiZnSb to be 0.292 C/m^2 under OCBC.

Furthermore, we also examine how another important HyFE quantity, namely the well depth (ΔF_{HyFE}) of the HyFE free energy under OCBC, depends on the inplane strain. The calculated ΔF_{HyFE} is shown in Fig.4(b), in comparison with the well depth ΔU_{FE} of ferroelectricity under SCBC. Fig.4(b) tells us that the absolute value of the HyFE free-energy well depth ΔF_{HyFE} increases with the compressive strain, varying from 0.32 eV at η=$-$1% to 0.55 eV at η=$-$6% [see the solid dots in Fig.4(b)]. This reveals that the HyFE instability can be effectively tuned by the inplane strain.

The discovery of a non-monotonous dependence of the HyFE polarization with the inplane strain in Fig.4(a) is interesting, and meanwhile, puzzling. We next provide a possible physical mechanism which leads to this unusual behavior. First we find that the decrease of P_{HyFE} from η=$-$1% to η=$-$3% is caused by the decrease in the mode effective charge $\widetilde{Z}_3$. $\widetilde{Z}_3$ of soft $A_{2u}(LO_1)$ phonon is given in Fig.4(c), showing that $\widetilde{Z}_3$ decreases significantly from η=$-$1% to η=$-$3%. Since the HyFE polarization is directly proportional to $\widetilde{Z}_3$, the decrease of $\widetilde{Z}_3$ thus leads to the decline of the HyFE polarization in the considered strain range. Considering that the Born effective charges are often valid only within the linear regime[47], we need be slightly cautious. To confirm our explanation, we compute the polarization P_{BEC} using the mode effective charge as $P_{BEC} = \frac{1}{\Omega}\widetilde{Z}_3 c\lambda_m$. We find that P_{BEC} indeed follows a similar non-monotonous behavior as the Berry-phase polarization P_{HyFE} in Fig.4(a), showing that our explanation is reasonable.

On the other hand, the increase of P_{HyFE} from η=$-$4% to η=$-$6% in Fig.4(a) can be attributed to the strain-induced increase of optimal λ_m (Note that λ_m is defined as the λ value where the electric free energy is at minimum). Fig.4(d) shows the optimal λ_m value as a function of inplane strain. From $-$1% to $-$3% strains, λ_m is similar and increases only slightly. However, when strain is varied from $-$4% to $-$6%, λ_m increases more drastically,

which gives rise to the enlarged HyFE polarization since P_{HyFE} is proportional to λ_m. This is indeed consistent with Fig.4(a) when strain varies from -4% to -6%.

Our finding on the strain dependence of hyperferroelectricity in LiZnSb could be technologically useful for the following reasons: (i) It reveals that the HyFE polarization can be effectively tuned by strains, despite the existence of strong depolarization field under OCBC. (ii) It also tells that the well depth of the HyFE free energy and HyFE instability can be considerably adjusted by inplane strain. This can be used to modify the Curie temperature for hyperferroelectricity. Furthermore, it may also be utilized to decrease the HyFE well depth, making the HyFE polarization easier to switch.

IV. CONCLUSIONS

A combination of three different methods—including the linear-response density-functional perturbation theory, the electric free-energy, and the modern theory of polarization—are used to investigate the hyperferroelectricity in LiZnSb. Furthermore, the strain dependence of the hyperferroelectric properties is also studied. Our main findings are summarized in the following.

(i) A giant hyperferroelectricity is discovered in LiZnSb. More specifically, in LiZnSb under -2% strain, the HyFE polarization under an open-circuit boundary condition is found to be 0.282 C/m^2, despite the existence of depolarization field. This magnitude of polarization under OCBC is ten times larger than most of the HyFE polarizations reported so far in other materials[1,13], and is in fact comparable to the ferroelectric polarization of prototypical bulk $BaTiO_3$ under SCBC (i.e., without the depolarization field). This giant HyFE polarization should open many technological applications of hyperferroelectricity.

(ii) The hyperferroelectricity in LiZnSb under OCBC is shown to be robust and remarkably stable. The well depth of free energy in LiZnSb under -2% strain is determined to be -332 meV. Note that this well depth is under OCBC, and its value is comparable to the FE well depth (-200 meV) of bulk $PbTiO_3$ under SCBC. Considering that the Curie temperature of bulk $PbTiO_3$ is T_C=493 °C, our result indicates that LiZnSb under OCBC is hyperferroelectric at room temperature.

(iii) The origin of the strong hyperferroelectricity in LiZnSb is found to come from two factors, both being important. One is the large mode effective charge of the soft $A_{2u}(LO_1)$

phonon, and the other is a large high-frequency dielectric constant ϵ_∞.

A large MEC of the soft $A_{2u}(LO_1)$ phonon is critical since it can produce a large HyFE polarization. In LiZnSb under -2% strain, $\widetilde{Z}_3$ of soft $A_{2u}(LO_1)$ phonon is calculated to be 2.59, which is more than 600% times larger than the value of 0.39 in another hyperferroelectric $LiNbO_3$. Since the HyFE polarization is directly proportional to $\widetilde{Z}_3$ of the soft LO phonon, a large MEC will thus lead to a large HyFE polarization.

Meanwhile, a large HyFE polarization often detrimentally gives rise to a strong depolarization field which tends to eliminate hyperferroelectricity. To maintain HyFE, large dielectric ϵ_∞ constant becomes necessary and important, since it reduces the depolarization energy [see Eq.(1)], and allows the well depth of electric free energy to be deep, thus stabilizing HyFE. Our calculations reveal that, when ϵ_∞ is reduced to 1/3 of its original value in LiZnSb, the free-energy well depth is drastically reduced by a factor of ten from ΔF=−332 meV to ΔF=−33.4 meV, showing that the HyFE instability is strongly suppressed. When ϵ_∞ is further reduced to 1/4 of its original value, HyFE completely disappears.

(iv) We further find that both the HyFE polarization and the HyFE free-energy well depth can be effectively tuned by inplane strain (Fig.4). This tunability allows us to adjust the HyFE well depth and polarization, depending on what is needed in practical applications. Moreover, we also reveal that the HyFE polarization responds to the inplane strain in a (considerably) different manner than the FE polarization. While the FE polarization in LiZnSb under SCBC shows a continuous increase with the increasing compressive strain, the HyFE polarization under OCBC nevertheless exhibits an interesting and non-monotonous strain dependence. Considering that hyperferroelectricity is an intriguing new phenomenon, we hope that the rich and interesting results obtained in this study will stimulate more theoretical and experimental interest in the field.

V. ACKNOWLEDGMENTS

This work was partially supported by the Office of Naval Research. Computations were performed on the computing facilities provided by the Arkansas High-Performance Computing Center, supported by NSF.

VI. APPENDIX

A. Electronic band structures and electric free energies of LiZnSb under different compressive inplane strains

In this Appendix, we describe in detail the calculated electronic band structures of centrosymmetric LiZnSb under different inplane strains, which are reported in Fig.5. Fig.5(a) reveals that, at -1% strain, a band gap clearly opens at Γ, showing that the system is an insulator, and therefore, both the Born effective charges and the electric polarization are well defined. When strain increases from -1% to -3%, Fig.5(b) and Fig.5(c) tell us that the band gap increases, and the gap is direct at the zone-center Γ point. As strain is further increased to -4%, the *local* conduction band minima (CBM) have similar energies at several $\vec{k}$ points, while the valence band maximum (VBM) remains at Γ [see Fig.5(d)]. When the strain continues to increase from -4% to -6%, Fig.5(e) and Fig.5(f) reveal that (i) the fundamental band gap in this strain range is no longer direct. More specifically, the CBM state changes from Γ to a $\vec{k}$ point between H and A, while the VBM state is still located at Γ. (ii) The fundamental band gap starts to decrease. Nevertheless, the system remains to have a finite band gap in the whole considered strain range (i.e., from -1% to -6%).

Fig.6 shows the electric free energy in LiZnSb under -1%, -3% and -5% strains, where the internal energy U and depolarization energy $U_{\rm dp}$ are also plotted. Fig.6 reveals that (i) the well depth of free energy becomes deeper as strain increases, and (ii) the depolarization energies of different inplane strains remain small and interestingly similar, since the high-frequency dielectric ϵ_∞ constant is high for all considered strains.

---

[1] K.F. Garrity, K.M. Rabe, and D. Vanderbilt, Hyperferroelectrics: Proper Ferroelectrics with Persistent Polarization, Phys. Rev. Lett. **112**, 127601 (2014).

[2] H. Fu, Physical constraint and its consequence for hyperferroelectrics, J. Appl. Phys. **116**, 164104 (2014).

[3] P. Li, X. Ren, G.-C. Guo, and L. He, The origin of hyperferroelectricity in $LiBO_3$ (B = V, Nb, Ta, Os), Sci. Rep. **6**, 34085 (2016).

[4] C.J. Fennie and K.M. Rabe, Ferroelectric transition in $YMnO_3$ from first principles, Phys. Rev. B **72**, 100103 (2005).

[5] E. Bousquet, M. Dawber, N. Stucki, C. Lichtensteiger, P. Hermet, S. Gariglio, J.-M. Triscone, and P. Ghosez, Improper ferroelectricity in perovskite oxide artificial superlattices, Nature (London) **452**, 732 (2008).

[6] N.A. Benedek and C.J. Fennie, Hybrid Improper Ferroelectricity: A Mechanism for Controllable Polarization-Magnetization Coupling, Phys. Rev. Lett. **106**, 107204 (2011).

[7] P. Chen, M.N. Grisolia, H.J. Zhao, O.E. Gonzalez-Vazquez, L. Bellaiche, M. Bibes, B.-G. Liu, and J. Iniguez, Energetics of oxygen-octahedra rotations in perovskite oxides from first principles, Phys. Rev. B **97**, 024113 (2018).

[8] M. Dawber, K.M. Rabe, and J.F. Scott, Physics of thin-film ferroelectric oxides, Rev. Mod. Phys. **77**, 1083 (2005).

[9] J. Junquera and P. Ghosez, Critical thickness for ferroelectricity in perovskite ultrathin films, Nature (London) **422**, 506 (2003).

[10] N.A. Benedek and M. Stengel, Polarization that Holds Steady, Physics **7**, 32 (2014).

[11] J.F. Scott and C.A. Paz de Araujo, Ferroelectric Memories, Science **246**, 1400 (1989).

[12] J.F. Scott, *Ferroelectric Memories* (Springer, Berlin, 2000).

[13] S. Qiu, L. Ma, S. Liu, and H. Fu, Possible existence of tristable polarization states in $LiNbO_3$ under an open-circuit boundary condition, Phys. Rev. B. **104**, 064112 (2021).

[14] S. Liu and R.E. Cohen, Origin of Negative Longitudinal Piezoelectric Effect, Phys. Rev. Lett. **119**, 207601 (2017).

[15] D. Du, P. J. Strohbeen, H. Paik, C. Zhang, K. T. Genser, K. M. Rabe, P. M. Voyles, D. G. Schlom, and J. K. Kawasaki, Control of polymorphism during epitaxial growth of hyperferroelectric candidate LiZnSb on GaSb (111)B, Journal of Vacuum Science and Technology B **38**, 022208 (2020).

[16] M. A. White, G. J. Miller, and J. Vela, Polytypism and Unique Site Preference in LiZnSb: A Superior Thermoelectric Reveals Its True Colors, J. Am. Chem. Soc. **138**, 14574 (2016).

[17] R. Adhikari and H. Fu, Hyperferroelectricity in ZnO: Evidence from analytic formulation and numerical calculations, Phys. Rev. B **99**, 104101 (2019).

[18] H. Fu and R.E. Cohen, Polarization rotation mechanism for ultrahigh electromechanical response in single-crystal piezoelectrics, Nature (London) **403**, 281 (2000).

[19] P. Hohenberg and W. Kohn, Inhomogeneous Electron Gas, Phys. Rev. **136**, B864 (1964); W. Kohn and L.J. Sham, Self-Consistent Equations Including Exchange and Correlation Effects, Phys. Rev. **140**, A1133 (1965).

[20] P. Giannozzi, S. Baroni, N. Bonini, M. Calandra, R. Car, C. Cavazzoni, D. Ceresoli, G.L. Chiarotti, M. Cococcioni, I. Dabo, A. Dal Corso, S. Fabris, G. Fratesi, S. de Gironcoli, R. Gebauer, U. Gerstmann, C. Gougoussis, A. Kokalj, M. Lazzeri, L. Martin-Samos, N. Marzari, F. Mauri, R. Mazzarello, S. Paolini, A. Pasquarello, L. Paulatto, C. Sbraccia, S. Scandolo, G. Sclauzero, A.P. Seitsonen, A. Smogunov, P. Umari, R.M. Wentzcovitch, QUANTUM ESPRESSO: a modular and open-source software project for quantum simulations of materials, J. Phys. Condens. Matter **21**, 395502 (2009).

[21] https://www.quantum-espresso.org.

[22] N. Troullier and J. L. Martins, Efficient pseudopotentials for plane-wave calculations, Phys. Rev. B **43**, 1993 (1991).

[23] The configurations for generating pseudopotentials are $1s^2 2p^{0.05}$ for Li, $3d^{10} 4s^1 4p^{0.1}$ for Zn, and $5s^2 5p^{2.5} 5d^{0.1}$ for Sb. The matching radii of pseudo-wavefunction and all-electron wavefunction are $r_{\rm cut}^{s,p}$ =1.5, 3.0 Bohr for Li, $r_{\rm cut}^{s,p,d}$ =2.0, 2.0, 2.5 Bohr for Zn, and $r_{\rm cut}^{s,p,d}$ =1.8, 1.8, 2.5 Bohr for Sb. The local channel of pseudopotential is chosen to be the screened Coulomb potential with r_c=1.30 Bohr for Li, the $4s$ pseudopotential for Zn, and the $5s$ pseudopotential for Sb.

[24] S. Baroni, S. Gironcoli, A. D. Corso, and P. Giannozzi, Phonons and related crystal properties from density-functional perturbation theory, Rev. Mod. Phys. **73**, 515-562 (2001).

[25] S. Baroni, P. Giannozzi, and T. Testa, Green's-function approach to linear response in solids, Phys. Rev. Lett. **58**, 1861 (1987).

[26] X. Gonze, Adiabatic density-functional perturbation theory, Phys. Rev. A **52**, 1096 (1995).

[27] X. Gonze and C. Lee, Dynamical matrices, Born effective charges, dielectric permittivity tensors, and interatomic force constants from density-functional perturbation theory, Phys. Rev. B **55**, 10355 (1997).

[28] M. Born and K. Huang, *Dynamical theory of crystal lattices* (Clarendon press, Oxford, 1988).

[29] M. Stengel, N. A. Spaldin, and D. Vanderbilt, Electric displacement as the fundamental variable in electronic-structure calculations, Nat. Phys. **5**, 304-308 (2009).

[30] R. D. King-Smith and D. Vanderbilt, Theory of polarization of crystalline solids, Phys. Rev. B **47**, 1651-1654 (1993).

[31] R. Resta, Macroscopic polarization in crystalline dielectrics: the geometric phase approach, Rev. Mod. Phys. **66**, 889-915 (1994).

[32] Y. Yao and H. Fu, Theory of the structure of electronic polarization and its strain dependence in ferroelectric perovskites, Phys. Rev. B **79**, 014103 (2009).

[33] J. W. Bennett, K. F. Garrity, K. M. Rabe, and D. Vanderbilt, Hexagonal ABC Semiconductors as Ferroelectrics, Phys. Rev. Lett. **109**, 167602 (2012).

[34] Dj. Guendouz, Z. Charifi, H. Baaziz, F. Soyalp, G. Ugur, and S. Ugur, Electronic structure, phase stability, vibrational and thermodynamic properties of the ternary Nowotny-Juza materials LiMgSb and LiZnSb, Physica B **519**, 39-52 (2017).

[35] A. Raeliarijaona and H. Fu, Mode sequence, frequency change of nonsoft phonons, and LO-TO splitting in strained tetragonal $BaTiO_3$ Phys. Rev. B **92**, 094303 (2015).

[36] H. Fu, Possible antiferroelectric-to-ferroelectric transition and metallic antiferroelectricity caused by charge doping in $PbZrO_3$ Phys. Rev. B **102**, 134118 (2020).

[37] R. E. Cohen, Origin of ferroelectricity in perovskite oxides, Nature (London) **358**, 136 (1992).

[38] We also compute the $\widetilde{Z}_3$ value for the soft transverse-optic $A_{2u}(TO_1)$ mode in LiZnSb (note that it is the soft TO mode), and the value is 3.98. The $\widetilde{Z}_3$ value of the soft LO mode is thus comparable to that of the soft TO mode.

[39] There are two mechanisms to generate hyperferroelectricity. The mechanisms for strong HyFE in LiZnSb and for weak HyFE in $LiNbO_3$ are rather different. In $LiNbO_3$ of weak HyFE, MEC is small, which leads to a small HyFE polarization and a small depolarization energy. In LiZnSb of strong HyFE, MEC is large, and ϵ_∞ need be large too.

[40] P. Yu and M. Cardona, *Fundamentals of Semiconductors* (Springer, Berlin, 1996).

[41] R. Xu, R. Gao, S. E. Reyes-Lillo, S. Saremi, Y. Dong, H. Lu, Z. Chen, X. Lu, Y. Qi, S.-L. Hsu, A. R. Damodaran, H. Zhou, J. B. Neaton, and L. W. Martin, Reducing Coercive-Field Scaling in Ferroelectric Thin Films via Orientation Control, ACS Nano. **12**, 4736 (2018).

[42] J. H. Haeni, P. Irvin, W. Chang, R. Uecker, P. Reiche, Y. L. Li, S. Choudhury, W. Tian, M. E. Hawley, B. Craigo, A. K. Tagantsev, X. Q. Pan, S. K. Streiffer, L. Q. Chen, S. W. Kirchoefer, J. Levy, and D. G. Schlom, Room-temperature ferroelectricity in strained $SrTiO_3$, Nature **430**, 758 (2004).

[43] C. Ederer and N.A. Spaldin, Effect of Epitaxial Strain on the Spontaneous Polarization of Thin Film Ferroelectrics, Phys. Rev. Lett. **95**, 257601 (2005).

[44] H. N. Lee, S. M. Nakhmanson, M. F. Chisholm, H. M. Christen, K. M. Rabe, and D. Vanderbilt, Suppressed Dependence of Polarization on Epitaxial Strain in Highly Polar Ferroelectrics, Phys. Rev. Lett. **98**, 217602 (2007).

[45] Y. Yao and H. Fu, Density-functional theory study of polarization saturation in strained ferroelectrics, Phys. Rev. B **80**, 035126 (2009).

[46] S. Dutta, P. Buragohain, S. Glinsek, C. Richter, H. Aramberri, H. Lu, U. Schroeder, E. Defay, A. Gruverman, and J. Iniguez, Piezoelectricity in hafnia, Nat. Commun. **12**, 7301 (2021).

[47] A. Chanana and U. V. Waghmare, Prediction of Coupled Electronic and Phononic Ferroelectricity in Strained 2D h-NbN: First-Principles Theoretical Analysis, Phys. Rev. Lett. **123**, 037601 (2019).

TABLE I: The lattice constants and atomic positions in the FE phase of LiZnSb. Atomis positions are given in the framework of lattice vectors, where one Li atom is placed at the origin. The second column is our results, and the third column is the results obtained in other studies.

Quantity	Our work	Others
a (Å)	4.355	4.376[a], 4.341[b]
c (Å)	7.073	7.081[a], 6.962[b]
Zn	(2/3, 1/3, 0.342)	(2/3, 1/3, 0.331)[a], (2/3, 1/3, 0.335)[b]
Sb	(1/3, 2/3, 0.224)	(1/3, 2/3, 0.212)[a], (1/3, 2/3, 0.217)[b]

[a]33, [b]34

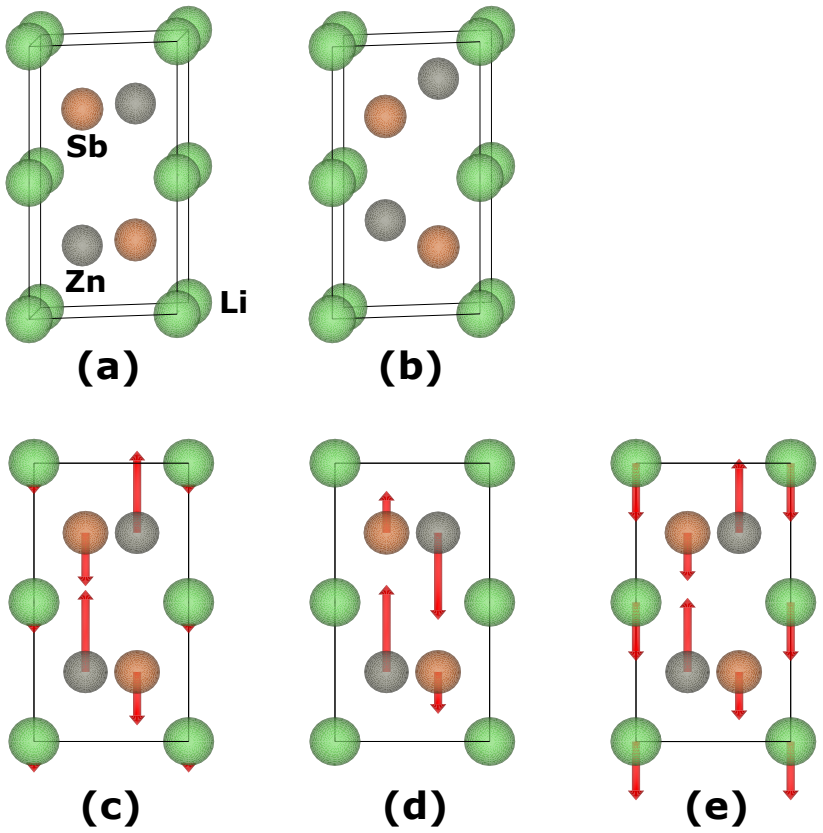

FIG. 1: (Color online) (a) A three-dimensional (3D) view of the unit cell of LiZnSb in the centrosymmetric PE phase; (b) A 3D view of the unit cell of LiZnSb in the FE phase. (c)-(e) The side views of the phonon eigenvectors of the following modes in PE LiZnSb under a -2% inplane strain: (c) soft transverse-optic $A_{2u}(TO_1)$ mode; (d) non-polar B_{1g} mode; (e) soft longitudinal-optic $A_{2u}(LO_1)$ mode. Atomic vibration amplitude and direction are shown in arrows. Li, Zn, and Sb atoms are shown respectively in green, gray, and golden colors.

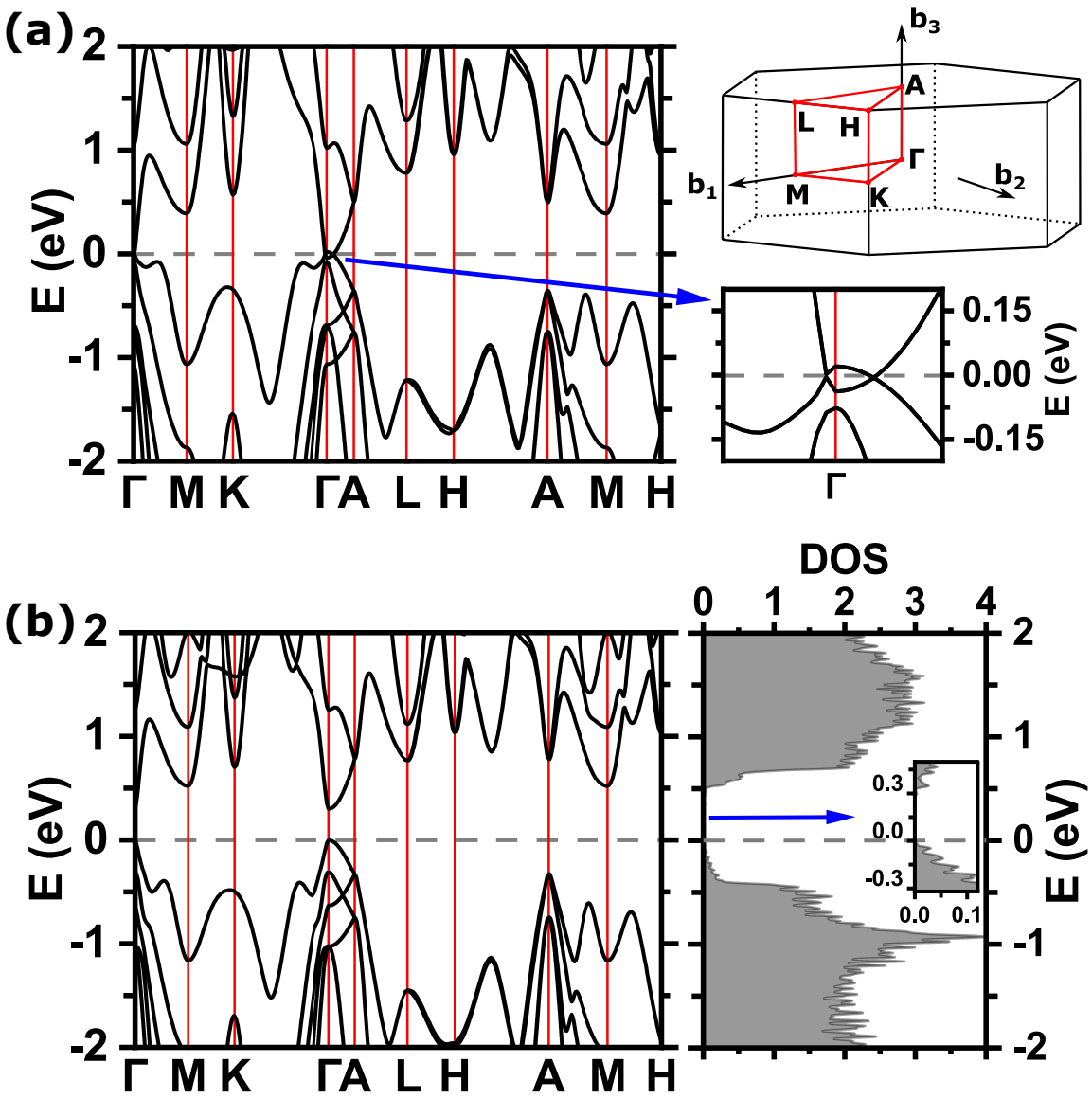

FIG. 2: Band structures of centrosymmetric (PE) LiZnSb under the following inplane strains: (a) under zero inplane strain, and (b) under a compressive -2% inplane strain. In (a), the band structure of unstrained LiZnSb is shown in the left; the enlarged band structure close to the Fermi level near Γ point is given in the bottom of the right. The Brillouin zone and high-symmetry points are given in the top of the right. In (b), the band structure of LiZnSb under a -2% inplane strain is shown in the left; the density of states (DOS) is given in the right (with the DOS near the band gap being enlarged in the inset).

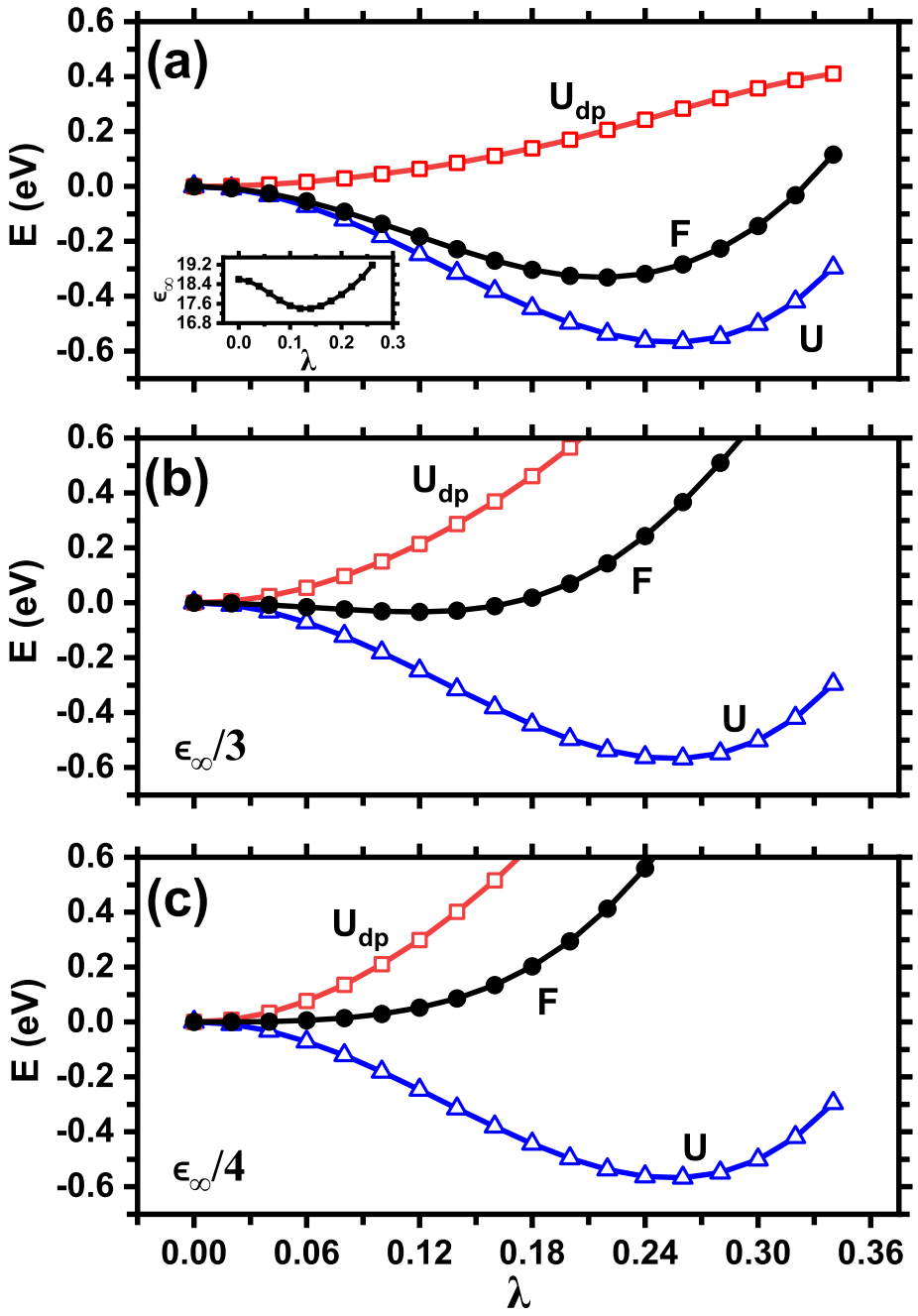

FIG. 3: (a) Electric free-energy $F(\lambda)$ (solid dots), internal energy $U(\lambda)$ (empty triangles), and depolarization energy $U_{dp}(\lambda)$ (empty squares) in -2% strained LiZnSb under OCBC as a function of λ. The calculated high-frequency dielectric constant $\epsilon_\infty(\lambda)$ is shown in the inset. (b) The same as (a), except that ϵ_∞ is artificially reduced to 1/3 of its original value. (c) The same as (a), except that ϵ_∞ is reduced to 1/4 of its original value.

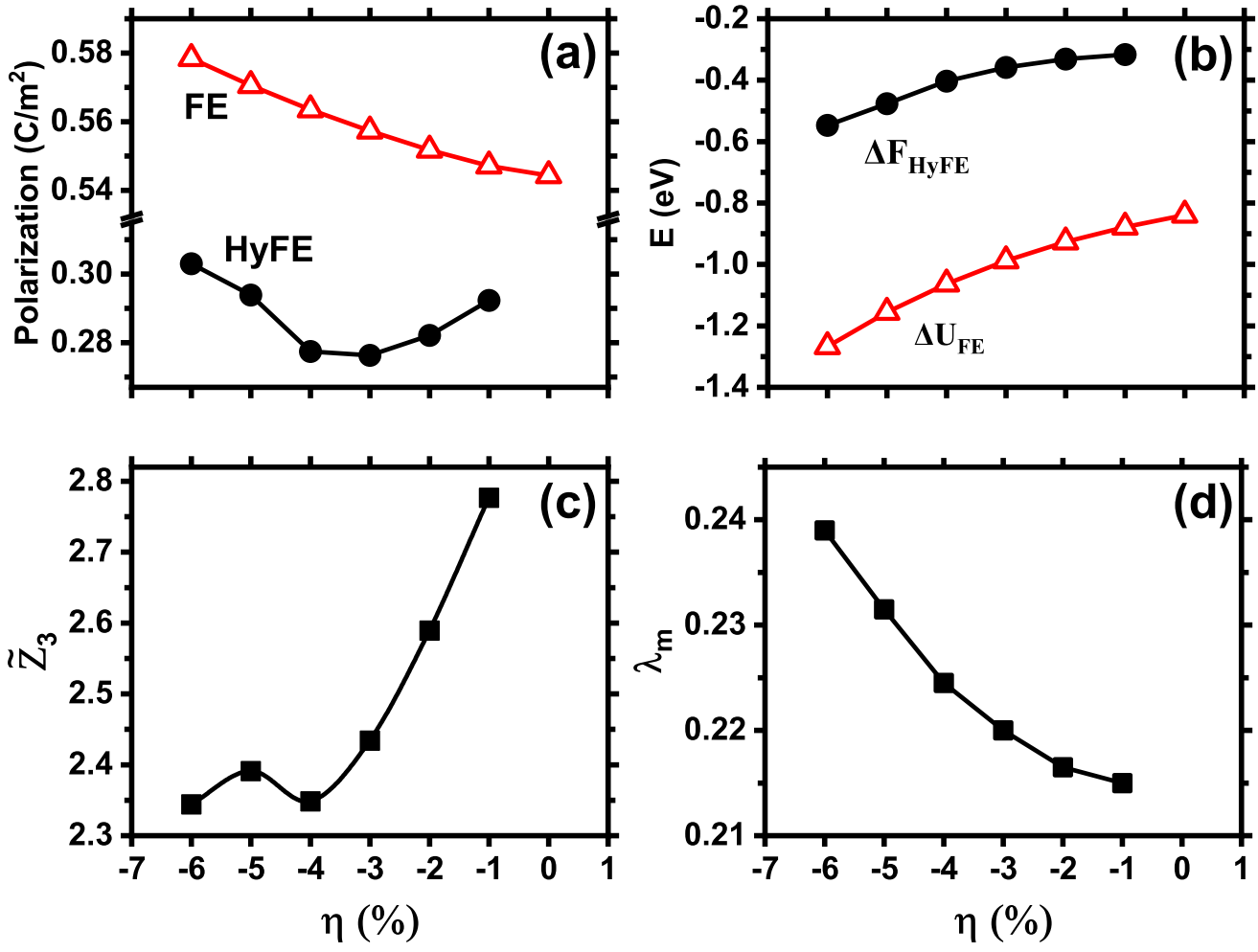

FIG. 4: The dependences of the following quantities in LiZnSb as a functions of the compressive inplane strain η: (a) The HyFE polarization under OCBC (solid dots) and the FE polarization under SCBC (empty triangles); (b) The free-energy well depth $\Delta F_{\rm HyFE}$ of hyperferroelectricity under OCBC (solid dots), and the internal-energy well depth $\Delta U_{\rm FE}$ of ferroelectricity under SCBC (empty triangles); (c) The mode-specific effective charge $\widetilde{Z}_3$ of $A_{2u}(LO_1)$ phonon; (d) The optimal λ_m.

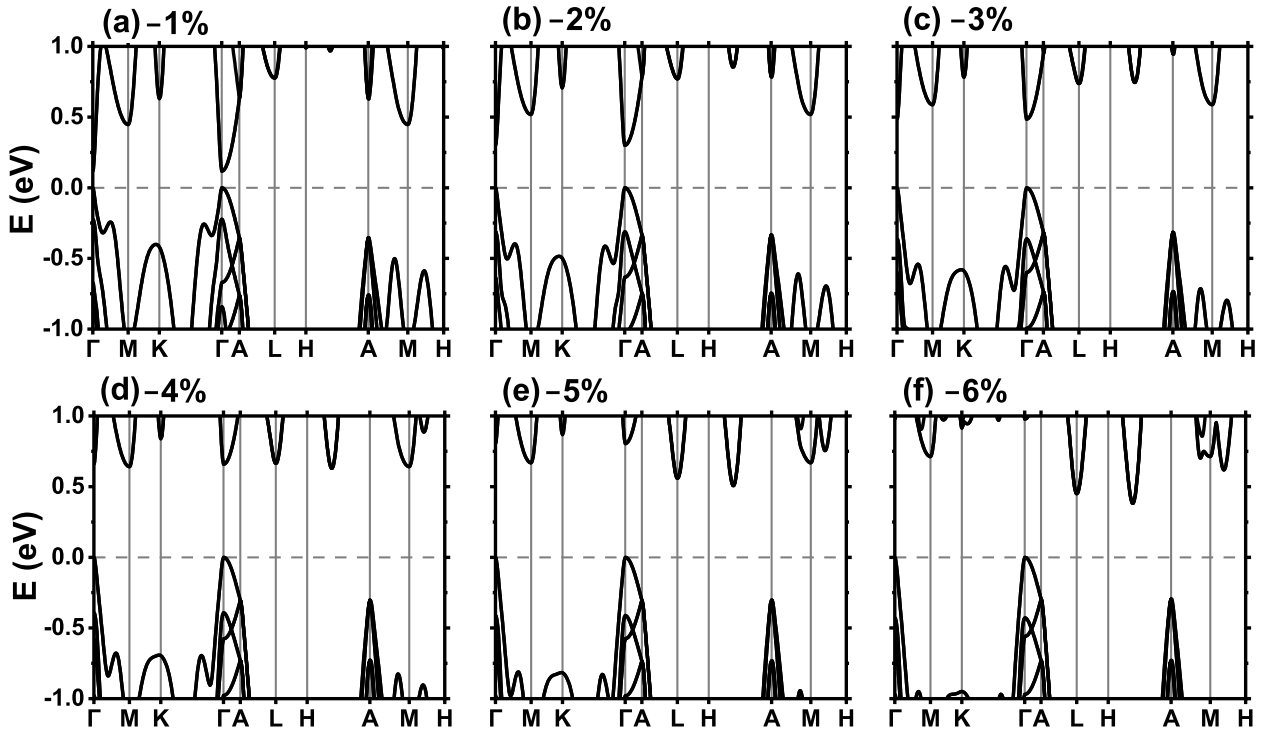

FIG. 5: Electronic band structure of centro-symmetric LiZnSb under the following compressive inplane strains: (a) −1%, (b) −2%, (c) −3%, (d) −4%, (e) −5%, and (f) −6%. The band gap is direct in (a)–(c), and becomes indirect in (d)–(f).

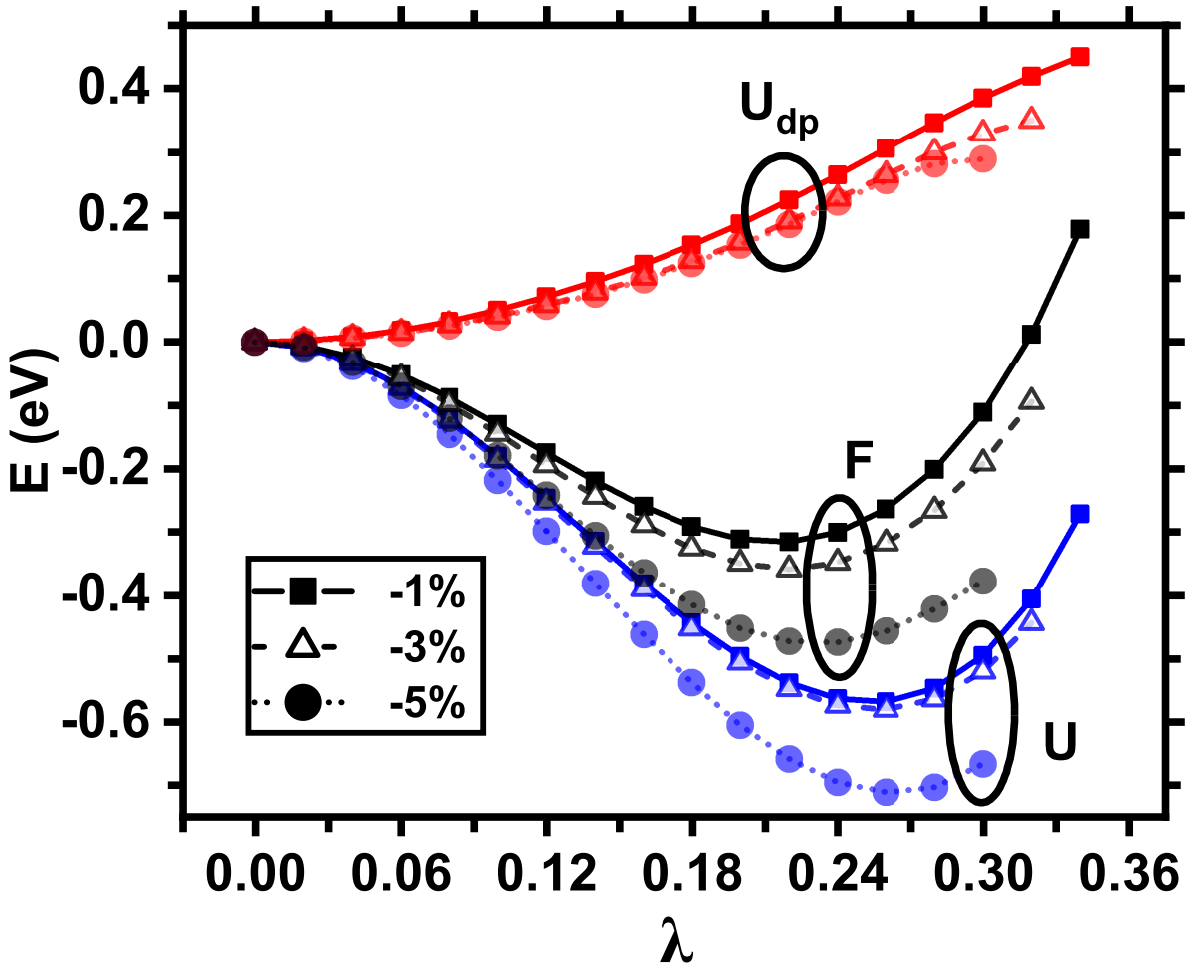

FIG. 6: (color online) Electric free-energy $F(\lambda)$ (marked as F) as a function of λ in strained LiZnSb under OCBC, for the following different inplane strains: -1% (solid squares), -3% (empty triangles), and -5% (solid circles). Internal energy $U(\lambda)$ (marked as U) and depolarization energy $U_{\rm dp}(\lambda)$ (marked as $\rm U_{dp}$) are also shown for comparison.